1 **Title: Emergent constraints on the sensitivity of global land surface runoff to temperature**

2 **based on CMIP6 projections**

3 **Authors**: Yuanfang Chai[1], Wouter R. Berghuijs[1], Yue Yao[2], Thomas A.J. Janssen[1] and Han

4 Dolman[1,3*]

5 [1] Department of Earth Sciences, Free University Amsterdam, Netherlands.

6 [2] State Key Laboratory of Water Resources and Hydropower Engineering Science, School of Water

7 Resources and Hydropower Engineering, Wuhan University, Wuhan, 430072 China

8 [3] School of Geography, Nanjing University of Science and Technology, Nanjing, China.

9 **Corresponding author:** Han Dolman

10 Address: Department of Earth Sciences, Free University Amsterdam, Netherlands.

11 Tel: +31-20-5987358

12 Email: han.dolman@vu.nl

13 ORCIDS: http://orcid.org/0000-0003-0099-0457

Key Points:

1. The uncertainty in future runoff sensitivity to temperature have been reduced by 7.2 – 12.0% using the emergent constraint method.

2. Applying an emergent constraint indicates original CMIP6 models underestimated future global runoff sensitivity to temperature by 36 – 104%.

3. Results indicate a shift towards a globally wetter climate.

Abstract: Climate change affects the water cycle. Despite the improved accuracy of simulations of historical temperature, precipitation and runoff in the latest Coupled Model Intercomparison Project Phase 6 (CMIP6), the uncertainty of the future sensitivity of global runoff to temperature remains large. Here, we identify an emergent relationship between the historical sensitivity of precipitation to temperature change (1979 – 2014) and the future sensitivity of runoff to temperature change (2015 – 2100), which can be used to constrain future runoff sensitivity estimates. Using this constraint, we estimate that the uncertainties in future sensitivity of runoff have been reduced by 7.2 – 12.0%. The constrained sensitivity of runoff is much larger (36 – 104%) than that directly inferred from original CMIP6 projections. Our constrained sensitivities also indicate more extreme wet conditions and fewer dry conditions. These results suggest that the future global land water cycle is accelerating and comes with more hydroclimatic extremes than previously projected.

31 **Plain language summary:** Climate change can affect river flow, which in turn affects the water

32 availability for society and the environment. However, how much global river flow will change due

33 to rising temperatures remains largely uncertain. A recently introduced methodology (the emergent

34 constraint) can reduce the uncertainties in anticipated future river flow change by using empirical

35 relationships between the current climate and the projected climate. After we apply this method to

36 the latest generation of Earth system models, we substantially reduce the uncertainty of future

37 projections, and the results suggests that land water cycle is accelerating faster and comes with a

38 more extreme wet and fewer extreme dry conditions than previously projected.

39

1 Introduction

Land surface runoff is changing with the global climate warming (Labat et al., 2004; Chai et al., 2020). These runoff changes can affect water availability for irrigation, hydropower generation, vegetation growth, industry and human use, especially in arid and semi-arid regions (Sorg et al., 2012). Thus, it is important to provide an accurate estimate of the feedback of future global runoff to rising temperatures. Such knowledge would not only help to better understand the effects of climate change on the terrestrial-water cycle, but could also assist in creating effective decision-making tools for water resources management and environmental protection (Rothausen et al., 2011).

There are however large uncertainties in the future effects of climate on global runoff, largely caused by poor simulation of rainfall and the inaccurate representations of the soil-plant-atmosphere system and human impacts (e.g. dams' operation and irrigation) in current Earth System Models (ESMs) (Du et al., 2016). Such uncertainties are sometimes to the extent that even the sign of the runoff change is unknown (Gedney et al., 2006; Piao et al., 2007; Shi et al., 2011). For the models included in the 5th generation Climate Model Intercomparison Project (CMIP5) (Taylor et al., 2012), the spread of global runoff across these models was rather large, as described in reports of the International Panel on Climate Change and several other studies (IPCC 2014; Alkama et al., 2013; Zhang et al., 2014; Yang et al., 2019). Compared to CMIP 5, the latest generation of ESMs (CMIP6) has increased both the vertical and horizontal spatial resolutions in the models, and includes more comprehensive numerical experimental designs and more detailed processes descriptions. (Meehl et al., 2014; Hall et al., 2019). Yet, the latest generation of ESMs (CMIP6) is still expected to have significant uncertainty in projecting the response of global runoff to a warming climate (Tokarska et

64   al., 2020; Wang et al., 2020).

65

66   An evaluation technique — the emergent constraint method (Hall et al., 2006), can reduce the

67   uncertainties of future climate projections, by using strong empirical relationships between current

68   climate and the projected future changes across a range of models (Wenzel et al., 2016, Cox et al.,

69   2013 and 2018; Sherwood et al., 2014;; Eyring et al., 2019; Terhaar et al., 2020; Chai et al., 2021). It

70   thereby offers perspective to also reduce the uncertainties in runoff projections under climate change

71   (Hall et al., 2019). A key challenge in introducing a new emergent constraint is the identification of

72   factor that dominates the uncertainties in global runoff sensitivity, and thereby allows constraining

73   projections of the future climate (Brient et al., 2020). In addition, the empirical relationship would

74   need to be grounded in a physical mechanism we understand (Brient et al., 2020). However, finding

75   such a climate factor can be difficult, because runoff changes in response to warming are affected by

76   many interrelated processes, including atmosphere, soil, and vegetation dynamics (Piao et al., 2007).

77

78   In this study, we aim to narrow the large spread of future runoff sensitivities ($\Delta R/\Delta T$) derived

79   from CMIP6 and CMIP5 simulations (Zhang et al., 2014). First, we evaluate the performance of 21

80   CMIP6 models' simulations of the historical climate by comparing them with both observations

81   (HadCRUT5) and CMIP5 simulations of temperature, precipitation and runoff for the period 1979 –

82   2014 (See details in SI 1). Subsequently, we assess the uncertainties in future $\Delta R/\Delta T$ during 2015 –

83   2100 both for CMIP6 models (under climate scenarios SSP126, SSP245, SSP370 and SSP585

84   (O'Neill et al., 2016)) and for CMIP5 models (under climate scenarios RCP26, RCP45, RCP60 and

85   RCP85 (Taylor et al., 2012)). We use the simulations of precipitation, evaporation, snow melt and

86 soil water content from these earth system model ensembles to infer a main cause of the trends in

87 future $\Delta R/\Delta T$. Identifying such a climate factor would enable to introduce a new emergent constraint

88 reduces the uncertainties of estimated $\Delta R/\Delta T$, under the condition that we find a strong relationship

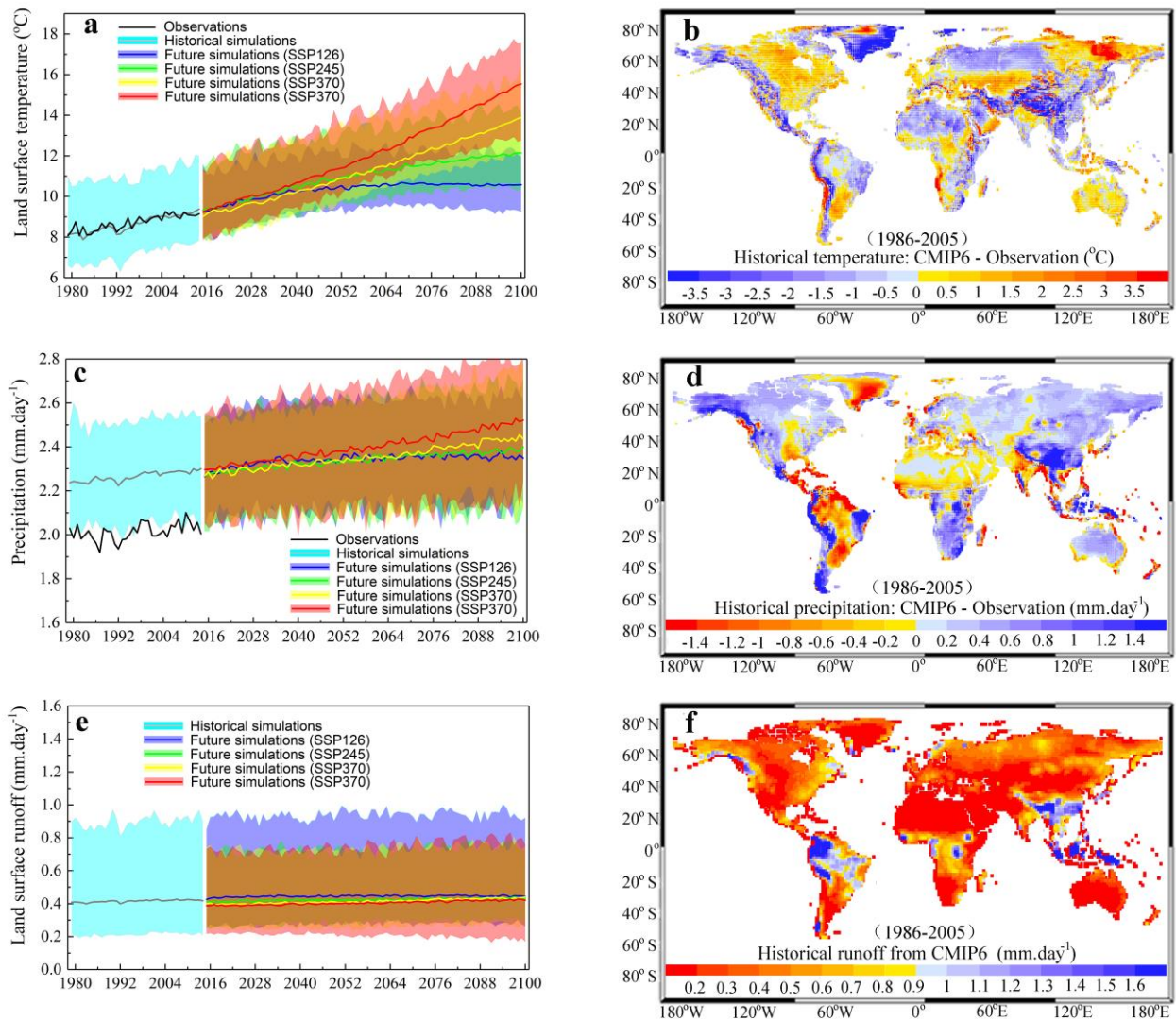89 between historical climate changes of the identified variable and future $\Delta R/\Delta T$.

90

91 **2 Performance of CMIP6 models**

92 **2.1 Temperature simulations**

93   The latest generation of CMIP6 models reproduce historical temperatures at both the regional

94 and the global scale better compared to the CMIP5 models (Figs. 1a and b and Fig. S1). CMIP6's

95 performance is weakest in some mountainous regions (e.g. the Himalayas and Andes) and high

96 latitude regions such as eastern Greenland and eastern Siberia (Fig. 1b), but the bias is smaller than

97 in CMIP5 models (Fig. S1). Similar to the previous-generations of ESM ensembles (Rogelj et al.,

98 2012; Keenan et al., 2018), the CMIP6 simulations project widespread warming under various

99 emission scenarios whereby temperatures are rising throughout the 21st century (Fig. 1a and Fig. S2).

100 The highest rates of surface warming are expected at high latitudes, due to polar amplification

101 (Stuecker et a., 2018; Biskaborn et al., 2019). Up to the year 2050, the global warming trends are

102 largely similar across the four emission scenarios (SSP126, SSP245, SSP370 and SSP585), while

103 after 2050 the projected temperatures diverge more clearly between the emission scenarios (Fig. 1a).

104 This divergence is caused by substantially lower CO_2 emissions after 2050 under SSP126 and

105 SSP245 compared to SSP370 and SSP585 (Gidden et al., 2019). Between the periods 2015 – 2024

106 and 2091 – 2100, the global land surface temperature is estimated to increase by 1.11 ± 0.52 °C (i.e.

107 mean ± standard deviation) under SSP126, up to 5.61 ± 1.08 °C under SSP585 (Fig. 1a). These

reported temperature increases are comparable with those in other studies that also use CMIP6 but

with slightly different ensembles (Cook et al., 2020; Fan et al., 2020; Tokarska et al., 2020).

Figure 1. CMIP6 simulations of global temperature (°C), precipitation (mm day^{-1}) and runoff (mm day^{-1}), and their comparison to the HadCRUT5 observational data set and CMIP5 simulations. Panels (**a**), (**c**) and (**e**) show the means and complete ensemble range of simulated trends in global mean temperature, precipitation and runoff based on CMIP6 models during 1979 – 2100 and in observations during 1979 – 2014, respectively. Panels (**b**) and (**d**) show the historical temperature and precipitation of CMIP6 minus the observed temperature and precipitation during 1986 – 2005. Panel (**f**) shows the CMIP6-based global distribution of runoff for the period of 1986 – 2005.

2.2 Precipitation simulations

CMIP6 models simulate historical precipitation better than CMIP5. Noticeable improvements

include the reduced underestimation of precipitation in southeastern China, India and South America

122   (Figs. 1c and d, Fig. S3). However, most CMIP6 models still considerably overestimate global

123   precipitation, whereby overestimations appear especially strong in several mountain regions (e.g. the

124   Himalayas and Andes), but to less extent than in CMIP5 projections (Fig. 1d and Fig. S3). Future

125   global precipitation is predicted to increase, especially in mountain regions, in major monsoon

126   regions, and at high latitudes (Fig. S4). Both these regional and global increases in precipitation are

127   consistent with projections of CMIP5 models (IPCC 2014). CMIP6 predicts future precipitation to

128   reduce mainly in large parts of South America, the Mediterranean, Southern Africa and Oceania,

129   which is also largely consistent with CMIP5. By the end of the 21st century (2091 – 2100), global

130   precipitation is projected to increase by 0.063 ± 0.023 mm day^{-1} (SSP126) up to 0.197 ± 0.065 mm

131   day^{-1} (SSP585) compared to 2015 – 2024.

132

133   **2.3 Land surface runoff simulations**

134   The CMIP6 historical runoff simulations (Fig. 1f) are significantly lower compared to the

135   observation-based Global Composite Runoff Fields from the Global Runoff Data Centre (Fig. S5)

136   (Fekete et al., 2002), but the underestimation of the global runoff is smaller than for CMIP5 (Fig. S6).

137   Models that are unable to reproduce past climate variations may have biases in their future climate

138   predictions (Klein et al., 2015). Therefore, the underestimation of historical runoff is likely to lead to

139   a underestimation of projections of future runoff. Underestimations of historical runoff are mainly

140   found in humid regions, including eastern North America, Europe, Southeast Asia, Central Africa,

141   and Indonesia. Such biases in modeled global runoff have also been reported in CMIP5 and are

142   likely largely the result of poor descriptions of precipitation, the soil-plant-atmosphere system and

143   human impacts (e.g. dams' operation and irrigation) (Du et al., 2016; Lehner et al., 2019). Global
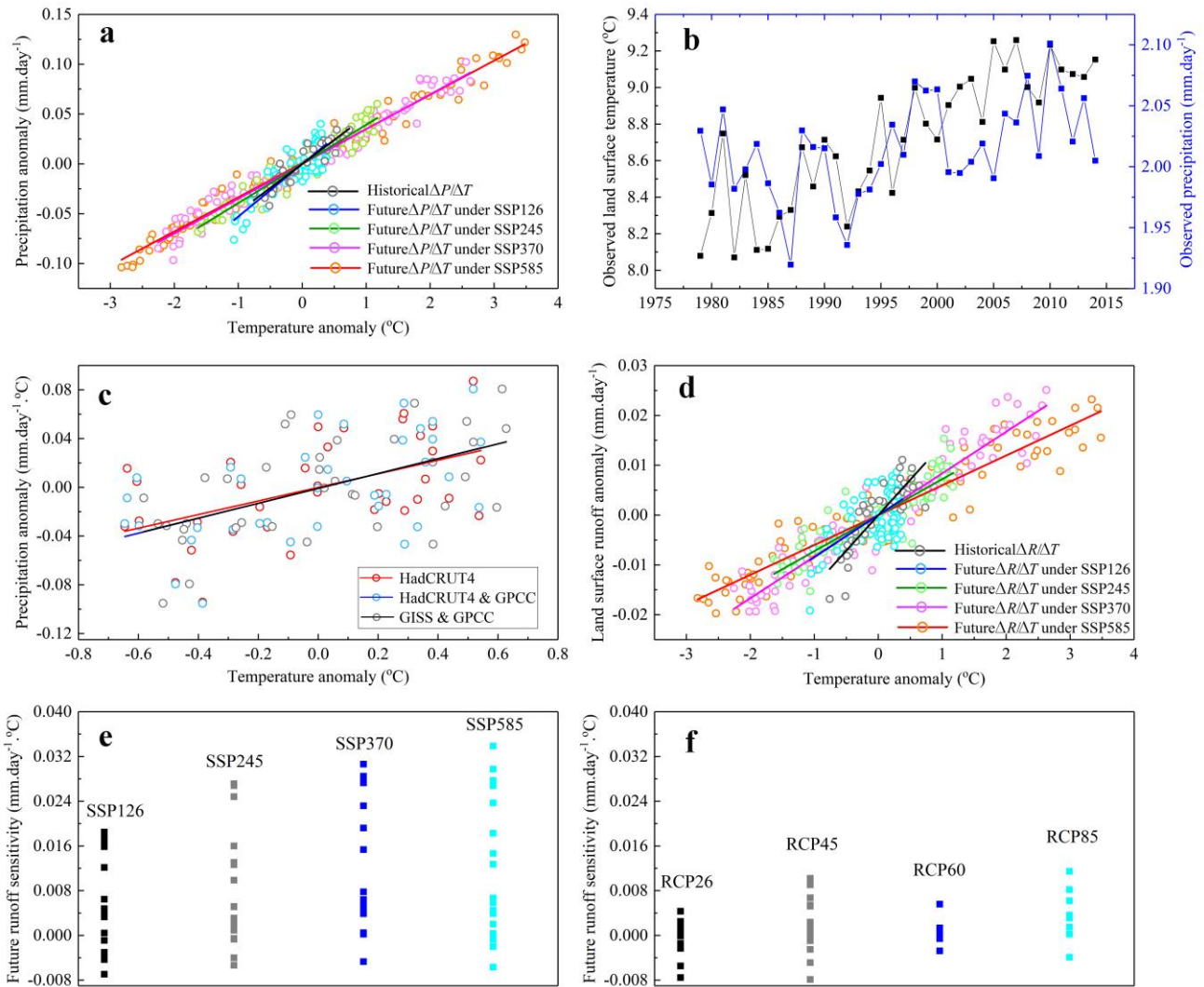
144 runoff is generally projected to increase over the 21st century (Fig. 1e). The estimated increase in

145 global runoff for the period of 2091 – 2100 compared to 2015 – 2024 ranges from 0.009 ± 0.009 mm

146 day^{-1} (SSP126) up to 0.035 ± 0.032 mm day^{-1} (SSP370), which equates to roughly a 2.25 ± 1.88% to

147 10.24 ± 10.91% increase. Especially East Asia, Central Africa and high northern latitudes show

148 strong increases in surface runoff over the 21st century (Fig. S7), which is consistent with the

149 projected precipitation increases in these same regions (Fig. S4). In contrast, future land surface

150 runoff is projected to decrease across largely parts of Europe, central North America, Southern

151 Africa, and the Amazon basin.

152

153 **3 Climate sensitivities**

154 **3.1 Global precipitation sensitivity to temperature**

155 CMIP6 models indicate that Earth's warming climate increases global precipitation (Figs. 1a

156 and c). The atmosphere can be expected to reduce its radiative energy under climate warming, which

157 would result in increased longwave emission due to higher temperatures (Previdi et al., 2010). To

158 obey conservation of energy, atmospheric latent heating would increase as an important

159 compensating process, which in turn would increase global precipitation (Liepert et al., 2009).

160 Because of these basic physical mechanisms, we hypothesize that a strong relationship between

161 global precipitation and global land surface temperature will exist. We indeed find a strong linear

162 relationship between precipitation and land surface temperature anomalies ($\Delta P/\Delta T$, mm day^{-1} °C^{-1}),

163 both for the historical simulations (r=0.95, p $value$<0.001) as well as the future projections (r≥0.98, p

164 $value$<0.001) (Fig. 2a and Fig. S8). The historical observations also have trends in global

165 precipitation and temperature that are synchronously rising (Fig. 2b). Linear estimates of $\Delta P/\Delta T$

166 using CMIP6, whether derived from the historical simulations (0.0482 mm day^{-1} °C^{-1}, Fig. 2a) or

derived from the future projections (0.0343 – 0.0528 mm day^{-1} °C^{-1}) are considerably lower than to

the linear estimates of $\Delta P/\Delta T$ derived from the three observational data sets (0.0557 – 0.0612 mm

day^{-1} °C^{-1}, Fig. 2c). Precipitation increases are expected to also increase in land surface runoff (e.g.,

Labat et al., 2004). Therefore, the likely underestimation of $\Delta P/\Delta T$ derived from CMIP6 simulations

may also cause an underestimation of $\Delta R/\Delta T$. This potential underestimation of $\Delta R/\Delta T$ is also

expected to be present in CMIP5 models, because they yield even lower $\Delta P/\Delta T$ estimates (0.0312 –

0.0550 mm day^{-1} °C^{-1}, Fig. S8) than CMIP6.

Figure. 2 Estimates of global $\Delta P/\Delta T$ (mm day^{-1} °C^{-1}) and global $\Delta R/\Delta T$ (mm day^{-1} °C^{-1}). Panel (**a**) shows the linear regression relations between annual average daily precipitation and annual average temperature based on CMIP6 outputs for the historical period of 1979 – 2014 ($P=0.0482T$, $r=0.93$, $p\ value<0.001$), and for the future

178 period of 2015 – 2100 under SSP126 ($P=0.0528T$, $r=0.88$, *p value*<0.001), SSP245 ($P=0.0393T$, $r=0.96$, *p*

179 *value*<0.001), SSP370 ($P=0.0348T$, $r=0.98$, *p value*<0.001) and SSP585 ($P=0.0343T$, $r=0.99$, *p value*<0.001).

180 Panel (**b**) shows the trends in the observed precipitation and temperature during 1979 – 2014 using HadCRUT5

181 data set. Panel (**c**) shows the observed $\Delta P/\Delta T$ during 1979 – 2014 using HadCRUT5 data set ($P=0.0557T$, $r=0.51$, *p*

182 *value*<0.001), HadCRUT5 – GPCC data set ($P=0.0612T$, $r=0.55$, *p value*<0.001) and GISS – GPCC data set

183 ($P=0.0609T$, $r=0.56$, *p value*<0.001). Panel (**d**) shows the linear regression relations between runoff and

184 temperature based on CMIP6 outputs for the historical period of 1979 – 2014 ($R=0.0142T$, $r=0.85$, *p value*<0.001),

185 and for the future period of 2015 – 2100 under SSP126 ($R=0.0085T$, $r=0.64$, *p value*<0.001), SSP245 ($R=0.0072T$,

186 $r=0.88$, *p value*<0.001), SSP370 ($R=0.0084T$, $r=0.95$, *p value*<0.001) and SSP585 ($R=0.0060T$, $r=0.95$, *p*

187 *value*<0.001). Panels (**e**) and (**f**) show the spread of $\Delta R/\Delta T$ across CMIP6 models and across CMIP5 models,

188 respectively.

189

190

191 **3.2 Global runoff sensitivities and their uncertainties**

192   Similar to the above-reported sensitivities of precipitation to temperature changes, we also find

193 a clear sensitivity of global runoff to temperature ($\Delta R/\Delta T$, mm day^{-1} $°C^{-1}$). This relation is something

194 to be expected because runoff tends to vary systematically with precipitation amounts. CMIP6

195 outputs exhibit a significant linear relationship between runoff and temperature (Fig. 2d), both in the

196 historical simulations ($r=0.85$, *p value*<0.001) as well as in the future projections ($0.64 \leq r \leq 0.95$, *p*

197 *values*<0.001), which corroborates the existence of a distinct global $\Delta R/\Delta T$. Positive relationships

198 between runoff and temperature also exist in CMIP5 models ($0.29 \leq r \leq 0.92$, *p values*<0.001; Fig. S9).

199 Using a similar approach as for the CMIP6 multi-model mean in Fig. 2d, we derived an estimate of

200 future global $\Delta R/\Delta T$ for each individual model (Fig. 2e). As expected, estimated $\Delta R/\Delta T$ relationships

201 show considerable variation across the CMIP6 models, to the extent that both positive and negative

202 sensitivities are estimated for a single emission scenario (Fig. 2e). A wide range of $\Delta R/\Delta T$

203 relationships are also visible in all RCP scenarios for the 5th generation of CMIP models (Fig. 2f),

204 but with narrower ranges than CMIP6 (possibly due to smaller climate sensitivity ($\Delta T/\Delta CO_2$) in

205 CMIP5 than in CMIP6). It should be noted that across all four emission scenarios the means of

206 estimated $\Delta R/\Delta T$ in CMIP6 (0.005 – 0.011 mm day^{-1} $°C^{-1}$) are higher than those of CMIP5 (-0.001 –

207 0.004 mm day^{-1} °C^{-1}). This again suggests that in general, the CMIP6 generation models show a

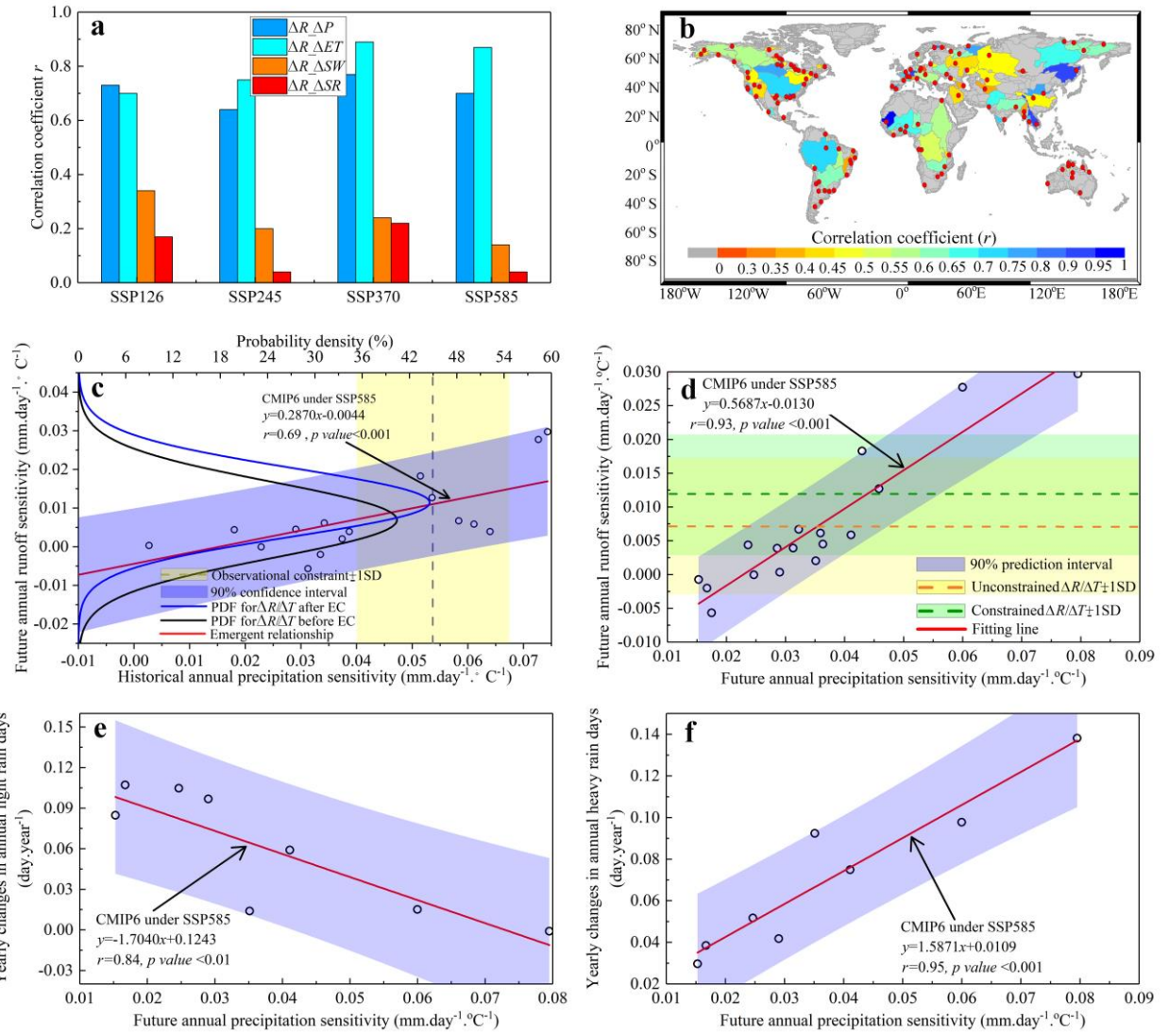208 smaller underestimation of the future runoff sensitivity compared to CMIP5.

209

210 **4 Emergent constraint**

211 **4.1 Physical mechanisms**

212   Identifying a dominant climatic factor that drives future runoff changes and its uncertainties is

213 key for increasing the confidence and understanding of the emergent constraint. Once this climatic

214 factor is identified, we can use observations of this climate factor to reduce the uncertainties in

215 estimated $\Delta R/\Delta T$. This is done by combing the empirical relationship between current variability in

216 this climatic factor and the future $\Delta R/\Delta T$ (See *SI 2.1* and *2.2* for details). The water balance dictates

217 that long-term changes in runoff depend on changes in precipitation, snow melt, soil water storage

218 and total evaporation (Lutz et al., 2014; Schoener et al., 2019). The last term, evaporation, is not only

219 driven by near-surface atmospheric conditions, but is also strongly modulated by physiological and

220 structural components of the vegetation (Gedney et al., 2006; Piao et al., 2007). Such complex

221 interacting mechanisms that can affect land surface runoff, might make it difficult to distinguish a

222 single main driving factor.

223

224   Through a simple linear regression analysis method we explored the factors contributing to

225 inter-model spread in estimated $\Delta R/\Delta T$ values. Such an approach has been earlier applied to

226 investigate the main drivers behind the changes in seasonal sea-ice albedo feedback (Thackeray et al.,

227 2019). The correlation coefficients of the linear relationships between future global runoff changes

228 and its potential main driving variables (Fig. 3a, and Fig. S10) show that both precipitation and total

229 evaporation exhibit a strong positive relationship with future runoff changes ($0.64 \leq r \leq 0.9$, *p*

230   *value*<0.001). On the contrary, changes in snow melt and soil water storage appear less important as

231   they show much weaker relationships with changes in global runoff ($0.04 \leq r \leq 0.34$, *p values*>0.1) (Fig.

232   3a). Spatially and temporally varying land surface conditions can make the drivers of regional runoff

233   changes more complex, but on global scale, the effects of precipitation and total evaporation change

234   appear far greater than the other factors. We note that increasing surface air temperatures can be

235   expected to result in a widespread increase in evaporation, which should logically result in a decline

236   of global runoff. However, the future global runoff is predicted to increase in both the CMIP6 and the

237   CMIP5 models. Therefore, we still identify precipitation as the dominant climatic factor affecting

238   changes in runoff that can be used for constraining future $\Delta R/\Delta T$. This constrained relation still holds

239   in the observations of 120 larger rivers as there are significant relations between the observed

240   precipitation and runoff (r>0.5 at 68% of the rivers, Fig. 3b), even though these rivers are strongly

241   affected by damming and other human influences (Nilsson et al., 2005). Because changes in

242   precipitation drive runoff changes, and are therefore both are similar in spatial and temporal

243   character, we expect that we can constrain the uncertainties in future $\Delta R/\Delta T$ using the historical

244    $\Delta P/\Delta T$ that we defined above (Fig. 2a).

245

Figure. 3 Emergent constraint on the future global $\Delta R/\Delta T$. Panel (**a**) shows the correlation coefficients r for the linear relations between the future runoff changes (ΔR) and the future changes in precipitation (ΔP), total evaporation (ΔET), soil water content (ΔSW) and snow melting runoff (ΔSR) respectively, from 2015 – 2024 to 2091 – 2100 based on CMIP6 projections. Panel (**b**) shows correlation coefficients r for the linear relations between the observed precipitation and the runoff in the 120 large rivers. Panel (**c**) shows the emergent constraint for the outputs from CMIP6 models under SSP585. Note: red line is the linear relationship between "the future global $\Delta R/\Delta T$ during 2015 – 2100 (see left y-axis)" and "the historical global $\Delta P/\Delta T$ during 1979 – 2014 (see bottom x-axis)"; yellow shading is the observational $\Delta P/\Delta T$ from the HadCRUT5 (0.056 ± 0.016 mm day^{-1} °C^{-1}). The blue shading is the 90% prediction error of the linear fitting; the black line and blue line are the probability density functions (PDFs, see top x-axis and left y-axis) for the future global $\Delta R/\Delta T$ before and after emergent constraint (*See SI 2.3* for more details); Panel (**d**) is the linear relationship between future $\Delta P/\Delta T$ and $\Delta R/\Delta T$ under SSP585. Note: The unconstrained and constrained $\Delta R/\Delta T$ under SSP585 are 0.007 ± 0.010 mm day^{-1} °C^{-1} and 0.0117 ± 0.0090 mm day^{-1} °C^{-1}, respectively. Panels (**e**) and (**f**) are linear relationships between $\Delta P/\Delta T$ and future yearly changes in global average annual light rainfall days, and between $\Delta P/\Delta T$ and future yearly changes in global average annual heavy rainfall days under SSP585. Note: See detailed trends in global average annual light and

261 heavy rainfall days in Fig. S11 and Fig. S12, respectively.

262

263 **4.2 Constrained runoff sensitivity**

264 Despite the relatively large variations in estimates of historical $\Delta P/\Delta T$ and future $\Delta R/\Delta T$ across

265 CMIP6 models (Fig. 2e), we still identify strong linear relationships between them across all

266 emission scenarios ($0.67 \leq r \leq 0.71$, *p values* < 0.001, Fig. 3c for SSP585, and Fig. S13 for SSP126,

267 SSP245 and SSP370). By using the observational $\Delta P/\Delta T$ from the HadCRUT5 dataset (yellow

268 shading in Fig. 3c), we find that most of the CMIP6 climate models lie outside the nominal

269 uncertainty bounds of the observational estimates. This may seem unexpected, but it has been shown

270 that most models do indeed show a systematic bias in their predictions (Klein et al., 2015). This

271 indicates that combining the empirical relationships of historical $\Delta P/\Delta T$ and future $\Delta R/\Delta T$, we can

272 constrain future $\Delta R/\Delta T$, by projecting the observed $\Delta P/\Delta T$ onto the vertical axis (Fig. 3c).

273

274 The constrained future $\Delta R/\Delta T$ increases for all emission scenarios (blue line in Fig. 3c and Fig.

275 S13) compared to the original CMIP6 outputs (black line). The original $\Delta R/\Delta T$ ranges from $0.005 \pm$

276 0.0082 mm day^{-1}.$°C^{-1}$ (SSP126) up to 0.009 ± 0.0092 mm day^{-1} $°C^{-1}$ (SSP370) (Table S7), whereas

277 the constrained estimates range from 0.0102 ± 0.0075 mm day^{-1} $°C^{-1}$ [1] (SSP126) up to $0.0122 \pm$

278 0.0081 mm day^{-1} $°C^{-1}$ (SSP370). This increase indicates that the future $\Delta R/\Delta T$ has been

279 underestimated in the multi-model means by $36 - 104\%$ ($0.0032 - 0.052$ mm day^{-1} $°C^{-1}$). Such a

280 significant range in underestimation by the CMIP6 original outputs is also present when using the

281 emergent constraint method with the other two observational data sets, where $\Delta R/\Delta T$ is

282 underestimated by $0.0043 - 0.0065$ mm day^{-1} $°C^{-1}$ (Fig. S14 and Table S7). Furthermore, the

283 constrained PDF of runoff sensitivity narrows compared to the unconstrained PDFs for all the

284 emission scenarios, which indicates that the inter-model spread in the future $\Delta R/\Delta T$ successfully

285 reduced after the emergent constraint. The reduced uncertainties are 8.5%, 7.2%, 12.0% and 10.0%

286 for the emission scenarios from SSP126 to SSP585 respectively. Similar strong empirical

287 relationships between historical $\Delta P/\Delta T$ and future $\Delta R/\Delta T$ also exist among CMIP5 models under

288 RCP26, RCP45, RCP60 and RCP85 ($0.34 \leq r \leq 0.71$, *p value* < 0.05, Fig. S15), which again increases

289 the estimates of future $\Delta R/\Delta T$ after applying the constraint. These results consistently show that our

290 introduced emergent constraint is valid and can be applied to constrain the models.

291

292   By multiplying the future increased multi-model mean temperature (ΔT) by the constrained

293 future $\Delta R/\Delta T$, we estimate the constrained future runoff changes in 2091 – 2100 relative to 2015 –

294 2024. Future runoff increases estimated using the constrain range from 0.0111 ± 0.0088 mm day^{-1}

295 (SSP126) up to 0.0656 ± 0.0504 mm day^{-1} (SSP585), which is much larger than those of the original

296 future runoff from CMIP6 models which range from 0.009 ± 0.009 mm day^{-1} (SSP126) up to $0.035 \pm$

297 0.032 mm day^{-1} (SSP370) (Table S7).

298

299 **4.3 Implications of the PDF shift**

300   The shift in PDFs of runoff sensitivity indicate that the probabilities of very low runoff

301 sensitivities are much smaller than in the original CMIP6 outputs (Fig. 3c,   Fig. S13 and Table S8).

302 The constrained sensitivities indicate it is more likely to be that runoff sensitivities are very high.

303 This suggests that global very wet conditions are more likely, and global very dry conditions more

304 rare. In addition, the future annual $\Delta P/\Delta T$ exhibit a tight positive linear relationship with the future

305 $\Delta R/\Delta T$ for each emissions scenario (Fig. 3d and Fig. S16). This positive relationship, combined with

306 the constrained future $\Delta R/\Delta T$, will shift the $\Delta P/\Delta T$ to a higher value by compared to the

307 unconstrained future $\Delta R/\Delta T$. Both results suggest there may be an underestimation in future $\Delta P/\Delta T$.

308 This again suggest that Earth's land surface may experience globally less dry conditions but more

309 extreme wet conditions in future compared to the original CMIP6 projections.

310

311   The expectation of more extreme wet conditions but fewer dry conditions is supported by

312 investigating the relationships between the future $\Delta P/\Delta T$ and the future yearly changes in both global

313 average annual light and heavy rain days (*See SI 2.4*). We find negative relations which indicate that

314 a model with a higher $\Delta P/\Delta T$ has a fewer global average annual light rainfall days (Fig. 3e and Fig.

315 S17). Thus, a potential underestimated $\Delta P/\Delta T$ (Fig. 3d) represents an overestimated frequency in

316 future global average light days. In contrast, future yearly increases in global average annual heavy

317 days exhibit a positive relationship with $\Delta P/\Delta T$ (Fig. 3f and Fig. S18). An underestimated $\Delta P/\Delta T$

318 moves the future yearly increase the number of global average annual heavy days. Using the

319 constrained future $\Delta R/\Delta T$ from the two other observed data sets (Table S7), we still reach the

320 conclusion that the future increases in global average light rainfall frequency has been overestimated

321 by the CMIP6 models outputs, while that for the global average heavy rainfall frequency has been

322 underestimated.

323

324 **5 Conclusions**

325   In this study, we find a strong physically-explainable empirical linear relationship between the

326 inter-model spread in the historical global $\Delta P/\Delta T$ and the inter-model spread in the future global

327 $\Delta R/\Delta T$ both for CMIP6 models and for CMIP5 models. This emergent constraint relationship allows

us to narrow the spread in future runoff sensitivities estimates from models. The constrained results reveal that sensitivities are much higher than those estimated directly from both the original CMIP6 and CMIP5 outputs. This implies that the land water cycle may be accelerating faster than suggested by the models' initial projections. The constrained estimates also suggest that future global climates will experience less global dry conditions but global more extreme wet conditions compared with the original CMIP6 projections. These implications for climates extremes are also supported by the CMIP6's overestimated future increases in global average annual light rainfall days and CMIP6's underestimated future increases in global average annual heavy rainfall days. We note that this result applies at the averaged global scale and is not necessarily opposed to the "dry regions get drier; wet regions get wetter" theorem that applies to the changes in the regional water cycle. Regional or continental scale feedbacks may still enhance the dryness parts of the globe. However, at the global scale the increased moisture holding capacity of the atmosphere leads to an accelerated hydrological cycle in which the Earth system overall is shifting towards a wetter state of the climate.

References

Alkama, R., Marchand, L., Ribes, A., & Decharme, B. (2013). Detection of global runoff changes: results from observations and CMIP5 experiments. *Hydrology and Earth System Sciences*, **17**(7), 2967. https://doi.org/10.5194/hess-17-2967-2013

Biskaborn, B. K., Smith, S. L., Noetzli, J., Matthes, H., Vieira, G., Streletskiy, D. A., et al. (2019). Permafrost is warming at a global scale. *Nature communications*, **10**(1), 1-11. https://doi.org/10.1038/s41467-018-08240-4

Brient, F. (2020). Reducing uncertainties in climate projections with emergent constraints: Concepts, Examples and Prospects. *Advances in Atmospheric Sciences*, **37**(1), 1-15. https://doi.org/10.1007/s00376-019-9140-8

Chai, Y., Yue, Y., Zhang, L., Miao, C., Borthwick, A.G., Zhu, B., et al. (2020). Homogenization and polarization of the seasonal water discharge of global rivers in response to climatic and anthropogenic effects. *Science of The Total Environment*, **709**, 136062. https://doi.org/10.1016/j.scitotenv.2019.136062

356   Chai, Y., Martins, G., Nobre, C., Randow, C., Chen, T., & Dolman, H. (2021). Constraining Amazonian land surface
357   temperature sensitivity to precipitation and the probability of forest dieback. *npj Climate Atmospheric*
358   *Science*, **4**, 6.
359   https://doi.org/10.1038/s41612-021-00162-1
360   Cook, B. I., Mankin, J. S., Marvel, K., Williams, A. P., Smerdon, J. E., & Anchukaitis, K. J., (2020). Twenty-first
361   century drought projections in the CMIP6 forcing scenarios. *Earth's Future*, **8**(6), e2019EF001461.
362   https://doi.org/10.1029/2019EF001461
363   Cox, P. M., Pearson, D., Booth, B. B., Friedlingstein, P., Huntingford, C., Jones, C. D., et al. (2013). Sensitivity of
364   tropical carbon to climate change constrained by carbon dioxide variability. *Nature*, **494**(7437), 341-344.
365   https://doi.org/10.1038/nature11882
366   Cox, P. M., Huntingford, C., & Williamson, M. S. (2018). Emergent constraint on equilibrium climate sensitivity
367   from global temperature variability. *Nature*, **553**(7688), 319-322.
368   https://doi.org/10.1038/nature25450
369   Du, E., Di Vittorio, A., & Collins, W. D. (2016). Evaluation of hydrologic components of community land model 4
370   and bias identification. *International journal of applied earth observation and geoinformation*, **48**, 5-16.
371   https://doi.org/10.1016/j.jag.2015.03.013
372   Eyring, V., Cox, P. M., Flato, G. M., Gleckler, P. J., Abramowitz, G., Caldwell, P., et al. (2019). Taking climate
373   model evaluation to the next level. *Nature Climate Change*, **9**(2), 102-110.
374   https://doi.org/10.1038/s41558-018-0355-y
375   Fan, X., Duan, Q., Shen, C., Wu, Y., & Xing, C. (2020). Global surface air temperatures in CMIP6: historical
376   performance and future changes. *Environmental Research Letters*, **15**(10), 104056.
377   https://doi.org/10.1088/1748-9326/abb051
378   Fekete, B. M., Vörösmarty, C. J., & Grabs, W. (2002). High-resolution fields of global runoff combining observed
379   river discharge and simulated water balances. *Global Biogeochemical Cycles*, **16**(3), 15-1.
380   https://doi.org/10.1029/1999GB001254
381   Gedney, N., Cox, P. M., Betts, R. A., Boucher, O., Huntingford, C., & Stott, P. A. (2006). Detection of a direct
382   carbon dioxide effect in continental river runoff records. *Nature*, **439**(7078), 835-838.
383   https://doi.org/10.1038/nature04504
384   Gidden, M. J., Riahi, K., Smith, S. J., Fujimori, S., Luderer, G., Kriegler, E., et al. (2019). Global emissions
385   pathways under different socioeconomic scenarios for use in CMIP6: a dataset of harmonized emissions
386   trajectories through the end of the century. *Geoscientific model development*, **12**(4), 1443-1475.
387   https://doi.org/10.5194/gmd-12-1443-2019
388   Hall, A., & Qu, X. (2006). Using the current seasonal cycle to constrain snow albedo feedback in future climate
389   change. *Geophysical Research Letters*, **33**(3), L03502.
390   https://doi.org/10.1029/2005GL025127
391   Hall, A., Cox, P., Huntingford, C., & Klein, S. (2019). Progressing emergent constraints on future climate
392   change. *Nature Climate Change*, **9**(4), 269-278.
393   https://doi.org/10.1038/s41558-019-0436-6
394   IPCC, 2014 Climate change (2014) synthesis report. Contribution of Working Groups I, II and III to the Fifth
395   Assessment Report of the Intergovernmental Panel on Climate Change [Core Writing Team, R.K. Pachauri and
396   L.A. Meyer (eds.)]. IPCC, Geneva, Switzerland
397   Keenan, T. F., & Riley, W. J. (2018). Greening of the land surface in the world's cold regions consistent with recent
398   warming. *Nature climate change*, **8**(9), 825-828.
399   https://doi.org/10.1038/s41558-018-0258-y

Klein, S. A., & Hall, A. (2015). Emergent constraints for cloud feedbacks. *Current Climate Change Reports*, **1**(4), 276-287.

https://doi.org/10.1007/s40641-015-0027-1

Kusunoki, S., & Arakawa, O. (2015). Are CMIP5 models better than CMIP3 models in simulating precipitation over East Asia?. *Journal of Climate*, **28**(14), 5601-5621.

https://doi.org/10.1175/JCLI-D-14-00585.1

Labat, D., Goddéris, Y., Probst, J. L., & Guyot, J. L. (2004). Evidence for global runoff increase related to climate warming. *Advances in water resources*, **27**(6), 631-642.

https://doi.org/10.1016/j.advwatres.2004.02.020

Lehner, F., Wood, A. W., Vano, J. A., Lawrence, D. M., Clark, M. P., & Mankin, J. S. (2019). The potential to reduce uncertainty in regional runoff projections from climate models. *Nature Climate Change*, **9**(12), 926-933.

https://doi.org/10.1038/s41558-019-0639-x

Liepert, B. G., & Previdi, M. (2009). Do models and observations disagree on the rainfall response to global warming?. *Journal of Climate*, **22**(11), 3156-3166.

https://doi.org/10.1175/2008JCLI2472.1

Lutz, A. F., Immerzeel, W. W., Shrestha, A. B., & Bierkens, M. F. P. (2014). Consistent increase in High Asia's runoff due to increasing glacier melt and precipitation. *Nature Climate Change*, **4**(7), 587-592.

https://doi.org/10.1038/nclimate2237

Meehl, G. A., Moss, R., Taylor, K. E., Eyring, V., Stouffer, R. J., Bony, S., et al. (2014). Climate model intercomparisons: Preparing for the next phase. *Eos, Transactions American Geophysical Union*, **95**(9), 77-78.

https://doi.org/10.1002/2014EO090001

Min, S. K., Zhang, X., Zwiers, F. W., & Hegerl, G. C. (2011). Human contribution to more-intense precipitation extremes. *Nature*, **470**(7334), 378-381.

https://doi.org/10.1038/nature09763

Neelin, J. D., Sahany, S., Stechmann, S. N., & Bernstein, D. N. (2017). Global warming precipitation accumulation increases above the current-climate cutoff scale. *Proceedings of the National Academy of Sciences*, **114**(6), 1258-1263.

https://doi.org/10.1073/pnas.1615333114

Nilsson, C., Reidy, C. A., Dynesius, M., & Revenga, C. (2005). Fragmentation and flow regulation of the world's large river systems. *Science*, **308**(5720), 405-408.

https://doi.org/10.1126/science.1107887

O'Neill, B. C., Tebaldi, C., Vuuren, D. P. V., Eyring, V., Friedlingstein, P., Hurtt, G., et al. (2016). The scenario model intercomparison project (ScenarioMIP) for CMIP6. *Geoscientific Model Development*, **9**(9), 3461-3482.

https://doi.org/10.5194/gmd-9-3461-2016

Piao, S., Friedlingstein, P., Ciais, P., de Noblet-Ducoudré, N., Labat, D., & Zaehle, S. (2007). Changes in climate and land use have a larger direct impact than rising CO_2 on global river runoff trends. *Proceedings of the National academy of Sciences*, **104**(39), 15242-15247.

https://doi.org/10.1073/pnas.0707213104

Previdi, M. (2010). Radiative feedbacks on global precipitation. *Environmental Research Letters*, **5**(2), 025211.

http://dx.doi.org/10.1088/1748-9326/5/2/025211

Rothausen, S. G., & Conway, D. (2011). Greenhouse-gas emissions from energy use in the water sector. *Nature Climate Change*, **1**(4), 210-219.

https://doi.org/10.1038/nclimate1147

443   Rogelj, J., Meinshausen, M., & Knutti, R. (2012). Global warming under old and new scenarios using IPCC climate
444   sensitivity range estimates. *Nature climate change*, **2**(4), 248-253.
445   https://doi.org/10.1038/nclimate1385

446   Schoener, G., & Stone, M. C. (2019). Impact of antecedent soil moisture on runoff from a semiarid
447   catchment. *Journal of Hydrology*, **569**, 627-636.
448   https://doi.org/10.1016/j.jhydrol.2018.12.025

449   Sherwood, S. C., Bony, S., & Dufresne, J. L. (2014). Spread in model climate sensitivity traced to atmospheric
450   convective mixing. *Nature*, **505**(7481), 37-42.
451   https://doi.org/10.1038/nature12829

452   Shi, X., Mao, J., Thornton, P. E., Hoffman, F. M., & Post, W. M. (2011). The impact of climate, CO_2, nitrogen
453   deposition and land use change on simulated contemporary global river flow. *Geophysical Research*
454   *Letters*, **38**(8), L08704.
455   https://doi.org/10.1029/2011GL046773

456   Sorg, A., Bolch, T., Stoffel, M., Solomina, O., & Beniston, M. (2012). Climate change impacts on glaciers and
457   runoff in Tien Shan (Central Asia). *Nature Climate Change*, **2**(10), 725-731.
458   https://doi.org/10.1038/nclimate1592

459   Stuecker, M. F., Bitz, C. M., Armour, K. C., Proistosescu, C., Kang, S. M., Xie, S. P., et al. (2018). Polar
460   amplification dominated by local forcing and feedbacks. *Nature Climate Change*, **8**(12), 1076-1081.
461   https://doi.org/10.1038/s41558-018-0339-y

462   Taylor, K. E., Stouffer, R. J., & Meehl, G. A. (2012). An overview of CMIP5 and the experiment design. *Bulletin of*
463   *the American meteorological Society*, **93**(4), 485-498.
464   https://doi.org/10.1175/BAMS-D-11-00094.1

465   Terhaar, J., Kwiatkowski, L., & Bopp, L. (2020). Emergent constraint on Arctic Ocean acidification in the
466   twenty-first century. *Nature*, **582**(7812), 379-383.
467   https://doi.org/10.1038/s41586-020-2360-3

468   Thackeray, C. W., & Hall, A. (2019). An emergent constraint on future Arctic sea-ice albedo feedback. *Nature*
469   *Climate Change*, **9**(12), 972-978.
470   https://doi.org/10.1038/s41558-019-0619-1

471   Tokarska, K. B., Stolpe, M. B., Sippel, S., Fischer, E. M., Smith, C. J., Lehner, F., et al. (2020). Past warming trend
472   constrains future warming in CMIP6 models. *Science Advances*, **6**(12), eaaz9549.
473   https://doi.org/10.1126/sciadv.aaz9549

474   Wang, Z., Zhan, C., Ning, L., & Guo, H. (2020). Evaluation of global terrestrial evapotranspiration in CMIP6
475   models. *Theoretical and Applied Climatology*, **143**, 521-531.
476   https://doi.org/10.1007/s00704-020-03437-4

477   Wenzel, S., Cox, P. M., Eyring, V., & Friedlingstein, P. (2016). Projected land photosynthesis constrained by
478   changes in the seasonal cycle of atmospheric CO_2. *Nature*, **538**(7626), 499-501.
479   https://doi.org/10.1038/nature19772

480   Yang, Y., Roderick, M. L., Zhang, S., McVicar, T. R., & Donohue, R. J. (2019). Hydrologic implications of
481   vegetation response to elevated CO_2 in climate projections. *Nature Climate Change*, **9**(1), 44-48.
482   https://doi.org/10.1038/s41558-018-0361-0

483   Yin, L., Fu, R., Shevliakova, E., & Dickinson, R. E. (2013). How well can CMIP5 simulate precipitation and its
484   controlling processes over tropical South America?. *Climate Dynamics*, **41**(11-12), 3127-3143.
485   https://doi.org/10.1007/s00382-012-1582-y

486 Zhang, X., Tang, Q., Zhang, X., & Lettenmaier, D. P. (2014). Runoff sensitivity to global mean temperature change
487   in the CMIP5 Models. *Geophysical Research Letters*, **41**(15), 5492-5498.
488   https://doi.org/10.1002/2014GL060382

489

Acknowledgements and Data Availability Statement

499

Author contributions

Yuanfang Chai and Han Dolman led the writing, designed the research and performed the data

analysis. Wouter R. Berghuijs, Yao Yue and Thomas A.J. Janssen provided valuable comments and

interpretation of results.

Code availability

The code for this study is available by request from the corresponding author.

Competing interests

The authors declare no competing interests.

Additional information

Correspondence and requests for materials should be addressed to Han Dolman.